

# DiG-Net: Enhancing Quality of Life through Hyper-Range Dynamic Gesture Recognition in Assistive Robotics

Eran Bamani Beer<sup>a,\*</sup>, Eden Nissinman<sup>b</sup>, Avishai Sintov<sup>b</sup>

<sup>a</sup>*Department of Mechanical Engineering, Massachusetts Institute of Technology (MIT), 77 Massachusetts Ave, Cambridge, 02139, MA, USA*

<sup>b</sup>*School of Mechanical Engineering, Tel-Aviv University, P.O. Box 39040, Tel-Aviv, 6997801, , Israel*

---

## Abstract

Dynamic hand gestures play a pivotal role in assistive human-robot interaction (HRI), facilitating intuitive, non-verbal communication, particularly for individuals with mobility constraints or those operating robots remotely. Current gesture recognition methods are mostly limited to short-range interactions, reducing their utility in scenarios demanding robust assistive communication from afar. In this paper, we introduce a novel approach designed specifically for assistive robotics, enabling dynamic gesture recognition at extended distances of up to 30 meters, thereby significantly improving accessibility and quality of life. Our proposed Distance-aware Gesture Network (DiG-Net) effectively combines Depth-Conditioned Deformable Alignment (DADA) blocks with Spatio-Temporal Graph modules, enabling robust processing and classification of gesture sequences captured under challenging conditions, including significant physical attenuation, reduced resolution, and dynamic gesture variations commonly experienced in real-world assistive environments. We further introduce the Radiometric Spatio-Temporal Depth Attenuation Loss (RSTDAL), shown to enhance learning and strengthen model robustness across varying distances. Our model demonstrates significant performance improvement over state-of-the-art gesture recognition frameworks, achieving a recognition accuracy of 97.3% on a diverse dataset with challenging hyper-range gestures. By effectively interpreting gestures from considerable distances, DiG-Net significantly enhances the usability of assistive robots

---

\*Corresponding author: eran0910@mit.edu

in home healthcare, industrial safety, and remote assistance scenarios, enabling seamless and intuitive interactions for users regardless of physical limitations.

*Keywords:* Dynamic Gesture Recognition, Assistive Robotics, Human-Robot Interaction, Hyper-Range Perception, Graph Transformer

---

## 1. Introduction

The growing number of individuals living with disabilities and requiring assistance has created a pressing demand for assistive technologies that enhance users’ independence, safety, and quality of life [1]. Among these, assistive robotic systems are increasingly integrated into environments where intuitive, nonverbal communication is essential for enabling natural interaction with individuals of varied abilities. Gesture-based interaction is particularly important in scenarios where speech is not an option. To contextualize our contribution, Table 1 presents a comparative overview of recent systems in this area, outlining their target users, sensing modalities, application domains, and level of human involvement. Our method is the only one to support dynamic gesture recognition at hyper-range distances, defined here as up to 30 meters, and to operate reliably in both indoor and outdoor environments, making it uniquely suited for real-world assistive deployment. Recent research has catalyzed a new generation of assistive systems capable of perceiving complex environments and interacting with humans in context-aware, natural ways [2, 3, 4]. Equally important, human-in-the-loop approaches are being developed to ensure these systems operate safely and reliably alongside people. These methods incorporate human feedback, predictive planning, and adaptive control to support trust and safety during close interactions [5, 6, 7]. To enable practical deployment, recent studies stress the importance of user-centered design and usability evaluation, ensuring assistive robots are intuitive, reliable, and effective [8, 9]. A key area of research supporting these goals is human-robot interaction (HRI), which focuses on enabling smooth, natural collaboration between people and robots, both in assistive contexts and everyday life [10, 11]. This reflects a broader shift from viewing robots as tools to recognizing them as partners that augment and support human capabilities [12].

Intuitive interaction mechanisms are essential to enable non-expert users to effectively communicate their intentions to robots. Hand and arm gestures are intuitive forms of nonverbal communication, widely used in daily human interactions, making them well-suited for HRI [23, 24, 25]. Gesture-based interactions reduce the need for complex verbal or physical interfaces, improve user experience, and

Table 1: Comparative Summary of Gesture-Based Assistive Robotics Systems

Paper	Population	Env	Modality	Application	Range	Human-in-the-Loop
Boboc et al. [13]	General users	Indoor	RGB-D	Home robot control	Short	Yes
Haseeb et al. [14]	Motor-impaired	Indoor	IMU	Head-based robot control	N/A	Yes
Rudigkeit et al. [15]	Tetraplegic	Indoor	IMU	Robot arm use	N/A	Yes
Yang et al. [16]	Upper-limb impaired	Indoor	EMG	Mobile manipulation	Long	Yes
Ababneh et al. [17]	Elderly, wheelchair	Indoor	RGB-D	Arm control via gesture	Short	Yes
Neto et al. [18]	Factory workers	Indoor	IMU	Assembly support	Mid	Partial
Werner et al. [19]	Elderly	Indoor	RGB-D	Bathing assistant	Short	Partial
Muñoz et al. [20]	Older adults	Indoor	RGB-D	Rehab & exercises	Short	Partial
Oudah et al. [21]	Speech-impaired elderly	Indoor	RGB-D	Emergency alerting	Mid	Yes
Bandara et al. [22]	Wheelchair users	Indoor	RGB-D	Wheelchair navigation	Short	Yes
This work	General users	Both	RGB	Remote HRI guidance	Hyper	Yes

allow for intuitive and rapid communication with robots, even for users with no technical expertise [26]. With gestures, a user can convey nonverbal and simple commands even from a long distance without the need to shout. For instance, a user may direct robot movements with pointing gestures [27].

Research in the field of gesture recognition has made significant progress, particularly in recognizing static gestures [28, 29, 30]. However, most gesture recognition approaches are limited to short-range interactions, typically within a few meters [31, 26, 24]. Moreover, gesture recognition methods, often described to be effective in the long range, are typically limited to around seven meters [32, 33]. However, this limitation hinders their applicability in real-world scenarios that demand longer-range HRI. Recognizing gestures from a truly long distance can significantly expand the potential applications of robots in environments such as public spaces, industrial settings, and emergencies, where natural, non-contact interactions are necessary [34, 35]. However, one of the key challenges in achieving effective long-range gesture recognition is the degradation of visual information due to factors such as reduced resolution, lighting variations, and occlusions [36, 37].

While our recent work [38] successfully demonstrated ultra-range recognition of static hand gestures using a simple web camera at distances up to 25 meters, recognizing dynamic gestures presents additional, significant challenges. Static gesture recognition relies primarily on spatial features captured in a single frame, whereas dynamic gesture recognition demands the extraction and analysis of temporal sequences across multiple frames, significantly increasing complexity due to motion blur, occlusions, and ambiguity between similar gestures. The transition from static to dynamic gestures represents a fundamental shift, requiring entirely new approaches rather than incremental extensions of existing methods. Dynamic

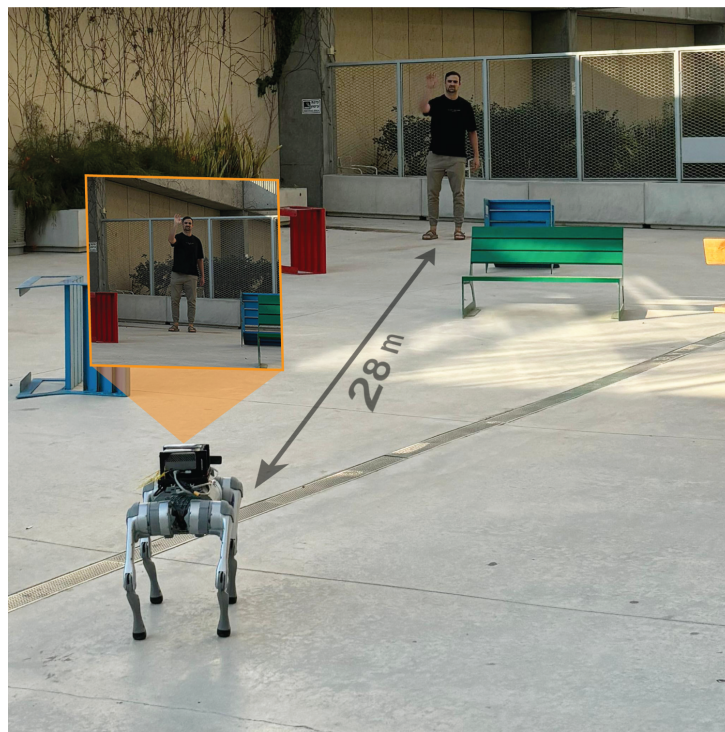


Figure 1: Demonstration of a user instructing a robot to go back by sweeping an open palm forward and backward, from a hyper-range distance. In addition to the low-resolution view of the user's hand, the robot may confuse the dynamic gesture with the static stop gesture.

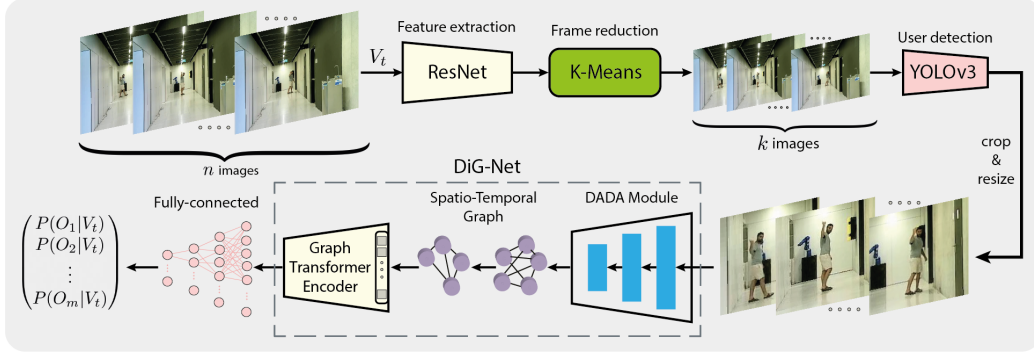


Figure 2: Overview of the proposed DiG-Net framework for Hyper-range dynamic hand gesture recognition. The framework starts with feature extraction using ResNet, followed by frame reduction using K-Means clustering. User detection is performed using YOLOv3, with the output frames resized to  $224 \times 224$ . The reduced frames are processed through the DiG-Net to robustly recognize gestures from RGB videos at distances up to 30 meters. The model integrates Depth-Conditioned Deformable Alignment (DADA), Spatio-Temporal Graph (STG) modules, and Graph Transformer encoders. Finally, a classification head is employed to acquire the gesture class.

gesture recognition at hyper-range presents a unique challenge that demands the fusion of spatial and temporal information across multiple scales and distances. At such long ranges, the visual signal of the performer is severely diminished, the region of interest occupies only a small portion of the frame, resulting in low-resolution observations, and environmental noise (e.g., background clutter, illumination changes, atmospheric effects) can significantly degrade each frame. In this scenario, temporal cues become as crucial as spatial cues for reliable recognition. Fast, subtle hand motions (e.g., a quick finger wave) might be nearly imperceptible in any single low-resolution frame, yet can be captured by analyzing differences across consecutive frames. Conversely, the overall spatial configuration of a gesture (e.g., an arm extended forward) may be visible but ambiguous without temporal context to distinguish its meaning. This interplay between space and time at extreme distances requires an architecture that can simultaneously capture fine, rapid movements and aggregate information over longer temporal intervals.

Dynamic gestures provide valuable context for understanding actions and systems, especially when explaining processes that unfold over time [39]. They are particularly effective for conveying spatial context to a task command [40]. For instance, a gesture instructing a robot to move backward would usually include an open palm swept back and forth toward it, as demonstrated in Figure 1. How-

ever, a snapshot of the gesture may be recognized as a static stop instruction if not processed correctly. Several studies have attempted to address dynamic gesture recognition by utilizing various data modalities. RGB-Depth (RGB-D) cameras are often used to recognize dynamic gestures but are limited to indoor environments [41, 42, 43, 44, 45]. Approaches using simple RGB cameras were also proposed while shown to function only indoors [32, 46, 47]. Table 2 summarizes the prominent work on dynamic gesture recognition with visual perception, highlighting the limitations of current approaches, which are typically restricted to indoor environments and short-range interactions (within 7 meters). In it also worth noting on-body sensors in wearable devices that instantly recognize hand gestures [48, 49]. While they can offer high recognition rates, wearable devices often require specialized and expensive hardware, limiting their accessibility to occasional users. Additionally, biometric approaches may not generalize well to new users, requiring additional data collection for each individual. On the other hand, visual perception allows for the observation of any user.

Table 2: State-of-the-art comparison of dynamic gesture recognition methods using visual perception

Paper	Camera	Range	Indoor	Outdoor
Zhou et al. [32]	RGB	$\leq 7m$	✓	✗
Xu et al. [41]	RGB-D	$< 1m$	✓	✗
Ma et al. [42]	RGB-D	$\leq 2m$	✓	✗
Kabir et al. [43]	RGB-D	$< 1m$	✓	✗
Bokstaller et al. [44]	RGB-D	-	✓	✗
Gao et al. [45]	RGB-D	$< 2m$	✓	✗
Yi et al. [46]	RGB	$\leq 6m$	✓	✗
dos Santos et al. [47]	RGB	-	✓	✗
Tran et al. [50]	5×RGB-D	$< 2m$	✓	✗
Wu et al. [51]	RGB-D	$< 2m$	✓	✗
Proposed method	RGB	$\leq 30m$	✓	✓

While the above methods show feasibility in controlled indoor settings, they often lack scalability and robustness for outdoor environments or hyper-range interactions. Their reliance on specialized hardware, such as a depth cameras, can increase cost and complexity, limiting their practical applicability [52]. Recent approaches utilizing multimodal data, including RGB, depth and human-pose (i.e., skeleton) information, have demonstrated potential for dynamic gesture recog-

dition [50, 51]. However, these methods are often also constrained by limited operational range and the need for specialized equipment. This makes them less suitable for scenarios requiring long-range interactions or deployment in large, open spaces. To the best of the authors’ knowledge, no work has addressed the problem of recognizing dynamic gestures at distances farther than seven meters.

In addition to capturing temporal features of dynamic gestures, the challenge is further compounded by the difficulty of perceiving spatial motions at far distances. In this paper, we address the problem of dynamic gesture recognition at hyper-range distance by only using a simple RGB camera. Specifically, we propose the Distance-aware Gesture Network (DiG-Net), illustrated in Figure 2, which comprises a novel Depth-Conditioned Deformable Alignment (DADA) block, seamlessly fused with Spatio-Temporal Graph (STG) modules [53]. Unlike existing approaches, DiG-Net adaptively warps feature maps based on per-pixel depth estimates to compensate for physical attenuation and defocus blur, while graph-based temporal modeling captures dynamic gesture patterns across frames. This unified design ensures robust feature alignment and temporal coherence, enabling accurate classification of subtle gestures at distances up to 30 meters under low-resolution and noisy conditions [54], which are common in hyper-range gesture recognition scenarios [37, 55].

To encourage the model to perform better at hyper-range distances, we introduce the Radiometric Spatio-Temporal Depth Attenuation Loss (RSTDAL). This specialized loss function incorporates both Beer–Lambert attenuation and defocus weighting to adaptively adjust each training sample’s contribution based on its distance from the camera, thereby strengthening recognition accuracy for gestures performed at greater distances. The proposed DiG-Net trained using the RSTDAL loss yields a robust and generalizable recognition for dynamic gestures in both indoor and outdoor environments. The model addresses key challenges in hyper-range gesture recognition, such as the degradation of visual information due to reduced resolution and lighting variations [56]. Furthermore, we introduce two novel metrics specifically designed to evaluate gesture recognition performance at long distances, including the stability of the recognition over time. Our approach is evaluated using these metrics, along with standard evaluation metrics.

To summarize, the key contributions of this work are:

- We propose the novel Distance-aware Gesture Network (DiG-Net), which comprises a novel Depth-Conditioned Deformable Alignment (DADA) block alongside Spatio-Temporal Graph modules to robustly capture spatial deformations and temporal dynamics of gestures at hyper-range distances.

- We introduce the Radiometric Spatio-Temporal Depth Attenuation Loss (RSTDAL), a specialized loss function incorporating Beer–Lambert attenuation and defocus weighting to improve recognition robustness across varying distances, enabling effective hyper-range gesture recognition.
- Unlike prior work, the proposed DiG-Net is the first to enable dynamic gesture recognition at hyper-range distances of up to 30 meters in both indoor and outdoor environments.
- We provide a comprehensive evaluation of our model against state-of-the-art gesture recognition frameworks, demonstrating superior performance in challenging hyper-range scenarios. The evaluation is conducted using novel metrics specifically designed for hyper-range gesture recognition.
- The trained models and datasets are publicly available to facilitate further research and development within the community<sup>1</sup>.

By enabling accurate dynamic gesture recognition at hyper-range distances, we significantly expand the potential applications of robots in environments such as public spaces, industrial settings, and emergency situations, where natural, non-contact interactions are necessary. Furthermore, our approach may enhance the ability of robots to interact with multiple users simultaneously, improving their utility in crowded or dynamic environments [57, 58]. Our method can also be applied in various fields, including search and rescue, drone operations and service robotics. Additionally, its applications may extend to space exploration, law enforcement and entertainment.

## 2. Methods

### 2.1. Problem Formulation

The primary objective of our work is for a robot to accurately recognize a human’s dynamic hand gestures at distances of up to 30 meters in diverse environments. Given a set of  $m$  gestures  $O_1, O_2, \dots, O_m$ , where each gesture can be either static or dynamic, the recognition task involves identifying the gesture performed in front of a simple RGB camera. The use of a standard RGB camera ensures that the dataset is applicable in real-world scenarios without the need

---

<sup>1</sup>To be available upon acceptance for publication.



for specialized hardware. Given an exhibited gesture  $O_j$  captured by the camera in a video sequence  $V_t = \{I_{t-n+1}, \dots, I_t\}$  of  $n$  past frames at time  $t$  ( $I_t$  is a video frame taken at time  $t$ ), we seek to maximize the conditional probability  $P(O_j | V_t)$ . Hence, our formulation aims to find  $O_{j^*}$  acquired from the solution of optimization problem

$$j^* = \underset{j}{\operatorname{argmax}} P(O_j | V_t), \quad j = 1, \dots, m. \quad (1)$$

Considering a sequence of past images enables the model to account for both the temporal and spatial dynamics of gestures, which is critical for differentiating between gestures that may appear similar when observed in a single frame.

## 2.2. Data Collection

To train a gesture recognition model, a comprehensive dataset of hand gestures is required. A video  $V_t$ , i.e., a sequence of images captured by a simple RGB camera, is given, showing a user exhibiting a gesture  $O_i$  at a distance  $\rho_i \leq 30$  m. The distance  $\rho_i$  was measured manually using a standard measuring tape during data collection and annotated per sample. This value remains fixed for the entire video sequence and is used during training, regardless of cropping or other pre-processing steps. This yields a dataset  $\mathcal{D} = \{(V_i, \rho_i, o_i)\}_{i=1}^N$  of  $N$  labeled video sequences, where  $o_i \in \{1, \dots, m\}$  is the gesture index. Figure 3 illustrates a diverse set of samples from the collected dataset, demonstrating the variety of environments, distances, and user poses used during data collection.

To enhance the dataset and improve the model’s generalizability, data augmentation techniques are applied to simulate various real-world conditions. These techniques included random cropping, horizontal flipping, rotation, scaling, brightness and contrast adjustments, and synthetic noise addition. These are aimed at simulating different camera positions, lighting conditions, viewing angles, and environmental challenges. The augmented dataset  $\tilde{\mathcal{D}} = \{(\tilde{V}_i, \rho_i, o_i)\}_{i=1}^M$  consists of both original and augmented video sequences, such that  $M > N$ . This enhanced dataset provides diverse training examples, thus improving the model’s robustness and performance under real-world variability.

## 2.3. Sequence Pre-processing

A sequence  $V_t$  contains  $n$  images, some of which may be highly similar, leading to redundancy. Hence, the sequences in  $\tilde{\mathcal{D}}$  are pre-processed to reduce the number of frames, resize them, and extract relevant features. Given a video  $V_t$ , the frames are reduced to  $r < n$  representative frames using K-Means clustering.

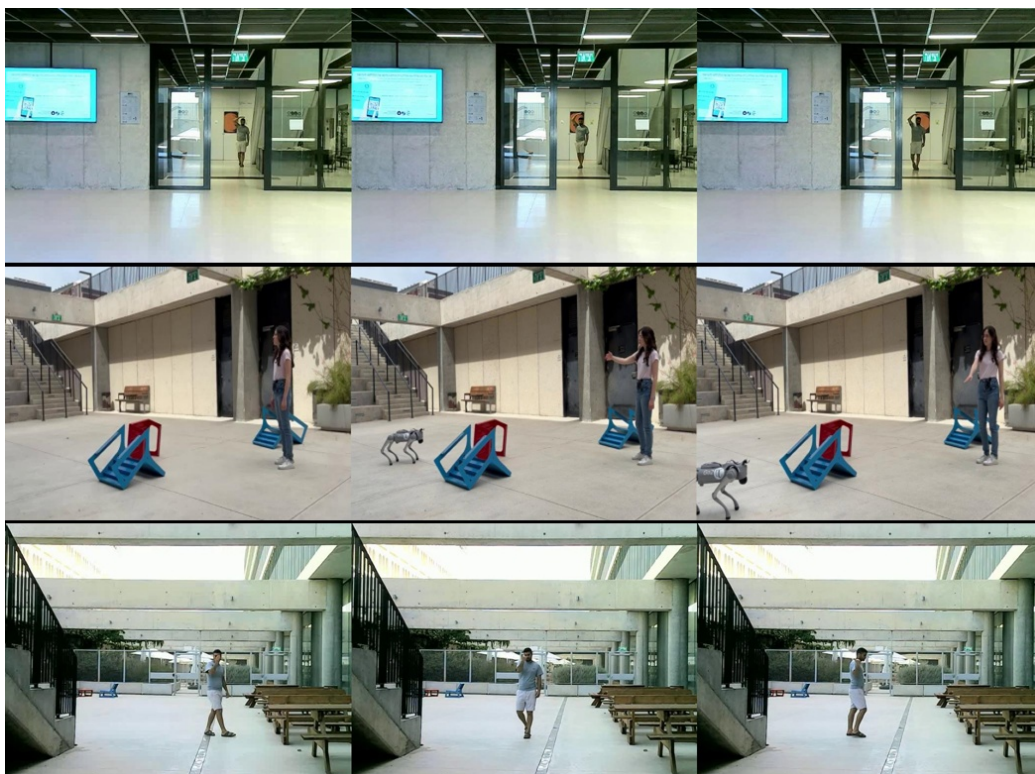


Figure 3: Example frames from the collected gesture dataset, showing different users, gestures, distances, and environments. The dataset includes both indoor and outdoor scenes with varying lighting and spatial arrangements to improve robustness and generalization.

Each frame  $\mathbf{I}_j \in V_t$  was processed through a pre-trained ResNet [59] to extract a low-dimensional feature vector  $\phi_j \in \mathbb{R}^d$ . All feature vectors were clustered into  $r$  clusters, and the frame corresponding to the feature vector closest to each cluster’s centroid was selected as the representative frame. In practice, a representative feature vector is chosen from cluster  $C_i = \{\phi_1, \phi_2, \dots\}$  according to

$$\text{rep}(i) = \arg \min_j \|\phi_j - \mathbf{C}_i\|_2, \quad (2)$$

yielding  $r$  representative frames  $\{\mathbf{I}_{\text{rep},1}, \mathbf{I}_{\text{rep},2}, \dots, \mathbf{I}_{\text{rep},r}\}$ . YOLOv3 [60] was then used to detect the user within each frame and crop the background, enhancing focus, particularly when the user was far from the camera. Full-body detection was chosen, as it provides more stable and consistent localization at hyper-range distances. In contrast, detecting small body parts like hands results in very limited regions, making the input noisier and less informative due to the loss of fine details. While YOLOv3 assists in isolating the user, it occasionally fails at long distances due to resolution loss. This emphasizes the importance of the model’s robustness in handling degraded inputs for reliable recognition. To address cases where the bounding box did not fully capture the human body, the bounding box was extended while maintaining a constant aspect ratio. Specifically, the pixel extension added around the bounding box was  $\frac{b}{a}$ , where  $b$  is the diagonal length of the bounding box, and  $a$  is a predefined user-to-image ratio parameter. The resulting cropped image was resized to  $224 \times 224$  pixels to ensure uniformity across the dataset, maintaining a consistent size and aspect ratio.

To stabilize the training process, the frames were also normalized to have zero mean and unit variance. In addition, optical flow was computed between consecutive frames to capture motion dynamics, providing information on the direction and magnitude of motion, which is essential for distinguishing between gestures with similar spatial features but different temporal movements. The optical flow data was used as an additional input channel alongside the RGB frames, providing both spatial and temporal information to the model. Dataset  $\tilde{\mathcal{D}}$  is updated to include the reduced and enhanced frames.

#### 2.4. DiG-Net Model Framework

The proposed DiG-Net integrates DADA blocks with STG modules and Graph Transformer encoders to robustly handle spatial distortions and temporal dynamics of hand gestures at hyper-range distances. Individually, DADA blocks effectively compensate for physical attenuation and defocus blur, but cannot capture

complex temporal dependencies. Conversely, STG modules and Graph Transformer encoders excel in modeling global spatio-temporal relationships but require well-aligned, noise-free inputs, making them sensitive to misalignment and distortions in low-resolution frames. DiG-Net addresses these complementary limitations by unifying depth-aware alignment, graph-based temporal reasoning, and global self-attention, thus enabling reliable recognition at distances of up to thirty meters. DiG-Net operates in a staged manner. Initially, input frames undergo successive DADA modules, which estimate motion-guided sampling offsets, perform ray-based feature warping, and correct for depth-related attenuation and defocus distortions. These depth-corrected features are then structured into a spatio-temporal graph, upon which the STG module executes spatial and temporal message passing to model local dynamics. Subsequently, Graph Transformer encoders apply multi-head self-attention across the graph nodes, effectively capturing long-range temporal dependencies and global contextual interactions. The self-attention mechanism of the Graph Transformer links early and late gesture phases, enhancing the importance of subtle deformation patterns identified through ray-sampling convolutions and resolving residual ambiguities inherent in distant, low-resolution inputs. Finally, the refined spatio-temporal features from the backbone network are concatenated into a tensor denoted by  $\mathbf{Y} \in \mathbb{R}^{B \times c_{\text{DADA}} \times T/4 \times H/4 \times W/4}$ , where  $B$  is the batch size,  $c_{\text{DADA}}$  represents the number of output channels after Graph Transformer processing, and  $T$ ,  $H$ , and  $W$  indicate the temporal length, spatial height, and spatial width of the input video sequence, respectively.

The initial feature map  $\mathbf{F}_0$  produced by the 3D convolutional stem is refined by the Motion–Depth Contextual OffsetNet, which predicts a dense offset field  $\Delta\mathbf{P}$  from the concatenation of  $\mathbf{F}_0$ , the per-pixel depth map  $z$ , and optical-flow channels  $(u, v)$ . This offset field guides the subsequent ray-sampling convolution, which warps  $\mathbf{F}_0$  along the local motion direction. Specifically, we first define the sampled feature  $\hat{\mathbf{F}}_0^{(k)} = \mathbf{F}_0(S_k(x, y, \tau))$ , where  $S_k(x, y, \tau)$  denotes the  $k$ -th sampling position along the normalized flow direction  $\hat{f}$ , scaled by  $k/z(x, y, \tau)$ , and is defined as

$$S_k(x, y, \tau) = (x, y) + \frac{k}{z(x, y, \tau)} \hat{f}, \quad \hat{f} = \frac{(u, v)}{\|(u, v)\| + \epsilon} \quad (3)$$

and  $(x, y)$  are spatial pixel coordinates,  $\tau$  is the frame index,  $k \in [-K, K]$  is the sampling offset index, and  $\epsilon$  a small constant for numerical stability. Subse-

quently, the warped feature map is defined as

$$F_{\text{warp}} = \sum_{k=-K}^K g_k(z(x, y, \tau), \|(u, v)\|) \hat{\mathbf{F}}_0^{(k)} \quad (4)$$

where  $g_k$  is a learned weighting function of depth and flow magnitude  $\|(u, v)\|$ . The warped features are then corrected for physical attenuation via

$$\mathbf{F}_{\text{corr}} = F_{\text{warp}} \exp(\eta z(x, y, \tau)) \quad (5)$$

with  $\eta$  the Beer–Lambert attenuation coefficient [61]. After spatio-temporal graph and Graph Transformer processing, the depth-corrected features are aggregated over space and time:

$$\mathbf{h}_i = \frac{1}{T'H'W'} \sum_{\tau=1}^{T'} \sum_{x=1}^{H'} \sum_{y=1}^{W'} \mathbf{F}_{\text{corr}}^{(i)}(x, y, \tau), \quad (6)$$

where  $T' = T/4$ ,  $H' = H/4$ , and  $W' = W/4$  denote the pooled temporal and spatial dimensions. The resulting vector  $\mathbf{h}_i \in \mathbb{R}^{\text{CDADA}}$  is then fed into a fully connected layer followed by Softmax to produce the final probability distribution  $\hat{\mathbf{y}}_i \in \mathbb{R}^m$ , where  $m$  is the total number of gesture classes.

To train the DiG-Net model, we propose the Radiometric Spatio-Temporal Depth Attenuation Loss (RSTDAL), a novel margin-based loss function tailored for robust gesture recognition at hyper-range distances. Unlike conventional loss functions that ignore distance-related degradations, RSTDAL incorporates depth-aware physical priors and motion dynamics to adaptively increase the decision margin for challenging inputs. Specifically, it penalizes the misclassification of gestures captured at far distances and with subtle motion, where attenuation and defocus effects severely degrade the signal. The loss function builds on an angular margin-softmax formulation, where the adaptive margin  $\mathcal{M}(\rho_i, \xi_i)$  is computed as:

$$\mathcal{M}(\rho_i, \xi_i) = \gamma_1(1 - e^{-\mu\rho_i}) + \gamma_2 Q + \gamma_3(1 - e^{-\lambda\xi_i}), \quad (7)$$

where  $Q = \left(1 - \frac{1}{1+(\rho_i/\rho_0)^2}\right)$  and  $\rho_i$  is the distance of the gesture,  $\xi_i$  is the average motion magnitude from the optical flow, and  $\mu, \rho_0, \lambda$  are learnable attenuation parameters. The overall RSTDAL loss is then given by:

$$\mathcal{L}_{\text{RSTDAL}} = -\frac{1}{B} \sum_{i=1}^B \log \frac{G}{G + \sum_{j \neq y_i} \exp(s \langle \mathbf{e}_i, \boldsymbol{\theta}_j \rangle)}, \quad (8)$$

where  $G = \exp(s(\langle \mathbf{e}_i, \boldsymbol{\theta}_{y_i} \rangle - \mathcal{M}(\rho_i, \xi_i)))$  and  $\mathbf{e}_i$  is the normalized embedding,  $\boldsymbol{\theta}_j$  are class prototypes,  $s$  is a scaling factor, and  $B$  is the batch size. By integrating distance, defocus, and motion terms into a unified margin, RSTDAL encourages better separation between classes under adverse visual conditions, significantly enhancing robustness across a wide range of distances and gesture speeds.

### 3. Model Evaluation

In this section, we evaluate the proposed DiG-Net framework for recognizing dynamic gestures used to naturally guide a robot. All computations were conducted on a Linux Ubuntu 18.04 LTS system equipped with an Intel Xeon Gold 6230R CPU (20 cores at 2.1 GHz) and four NVIDIA GeForce RTX 2080TI GPUs, each with 11 GB of RAM. Hyperparameter tuning was performed using Ray-Tune [62] to all models.

#### 3.1. Gestures

The evaluation focuses on  $m = 13$  distinct gesture classes. Of the 13, eight are dynamic, seen in Figure 4, and include: *go-back* with a forward and backward motion of an open hand, palm facing outward; *go-up* with an upward motion of an open hand, palm facing upward; *go-down* with a downward motion of an open hand, palm facing downward; *move-right* with a horizontal sweeping motion of the open hand, palm facing right; *move-left* with horizontal sweeping motion of the open hand, palm facing left; *turn-around* with a circular motion of the index finger, pointing upwards; *beckoning* where the palm is facing upward and the fingers are rhythmically flexed and extended; *follow-me* where the open palm is repeatedly tapped on the head of the user.

Another four static gestures are included: *pointing*, *thumbs-up*, *thumbs-down*, and *stop*. These gestures were chosen due to their mainstream usage and to challenge our model. That is, confusion between static and dynamic gestures may occur, such as in turn-around vs. pointing, go-back vs. stop, and go-up vs. beckoning. All gestures can be performed with either the left or right arm. The last class is the *null*, which represents the absence of any exhibited gesture, in which the user can perform any unrelated activities.

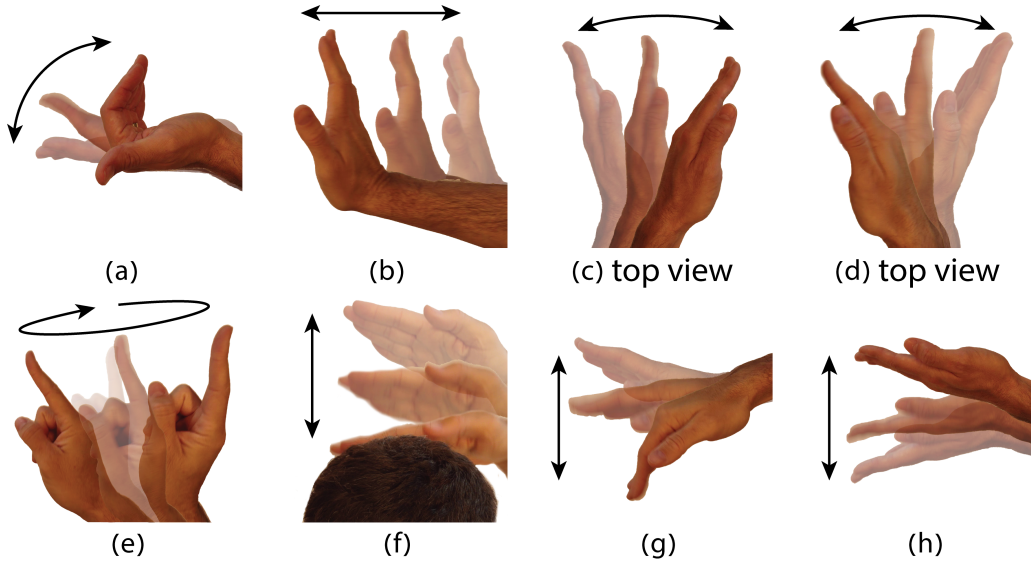


Figure 4: The eight dynamic gestures used in the analysis include: (a) beckoning, (b) go-back, (c) move-right, (d) move-left, (e) turn-around, (f) follow-me, (g) go-down and (h) go-up.

### 3.2. Dataset

Dataset  $\mathcal{D}$  was collected by recording video samples of the  $m = 13$  gestures at a distance range of  $\rho \in [2, 30]$ . Gestures were exhibited in diverse environments, including both indoor and outdoor settings, varying lighting, and diverse backgrounds. In addition, 16 different participants contributed gesture data to ensure variability in gesture performance. Each participant performed each gesture multiple times at different measured distances. The data collection process involved using a standard RGB camera with a resolution of  $640 \times 480$  pixels taken at 21 frames per second. Each gesture was manually annotated according to its class  $o_i$  and the distance  $\rho_i$  at which it was performed, resulting in labeled data suitable for supervised learning. This annotation allowed for a detailed analysis of model performance across varying distances, as well as the development of distance-specific recognition strategies. The collected dataset  $\mathcal{D}$  yielded  $N = 3,240$  video samples of hand gestures, each lasting 4 seconds with up to  $n = 84$  frames. After feature extraction as described in Section 2.3, the number of frames was reduced to  $k = 8$  per video. With further augmentation, dataset  $\tilde{\mathcal{D}}$  includes  $M = 4,790$  samples. An additional test set of  $K = 458$  labeled and processed videos was recorded in distinct environments to evaluate the model’s performance.

### 3.3. Comparative Evaluation

We now evaluate the proposed DiG-Net model compared to existing state-of-the-art gesture recognition frameworks. The DiG-Net model was trained with the Lion optimizer [63], chosen for its efficiency and convergence stability, using an initial learning rate of 0.0037. The learning rate was gradually reduced using a cosine annealing schedule to ensure stable convergence. The model was trained for 100 epochs with a batch size of  $B = 16$ , using the proposed RSTDAL loss function (8), which adaptively adjusts the angular margin based on the gesture distance  $\rho_i \in [2, 30]$  and motion magnitude  $\xi_i$  through the learnable function  $\mathcal{M}(\rho_i, \xi_i)$ . The margin function incorporated fixed attenuation parameters of  $\mu = 0.1$  and  $\lambda = 0.2$ , with a reference distance  $\rho_0 = 16$  used in the non-linear margin term to center the response. The weights of the three margin components were set to  $\gamma_1 = 0.4$ ,  $\gamma_2 = 0.5$ , and  $\gamma_3 = 0.2$ , respectively, to balance the influence of exponential decay over distance, the non-linear reference curve, and motion magnitude. These hyperparameters were optimized using RayTune [64] to balance the emphasis on long-range samples and ensure stable training. To prevent overfitting, dropout was applied at the output of the Graph Transformer encoder, and L2 regularization was used during training. Early stopping was employed by monitoring the validation loss to determine the optimal stopping epoch. The DiG-Net model is compared to the: Swin Transformer [65] which uses shifted windows for efficient spatial feature extraction; ViViT [66], a Transformer for video analysis capturing spatial and temporal relationships; TimeSformer [67] which separates temporal and spatial attention; MViT [68], a multiscale Transformer for spatiotemporal resolutions; I3D [69], a 3D convolutional network for spatiotemporal learning; and, X3D [70], an efficient 3D convolutional model balancing speed and accuracy.

The models were trained and evaluated on the same datasets to ensure a fair comparison. We employ five key metrics: recognition success rate, Mean Average Precision (mAP),  $F_1$  Score, Distance-Weighted Accuracy (DWA), and Gesture Stability Score (GSS). While the three former ones are common metrics, we propose to include the latter two for a comprehensive evaluation across distances and their consistency over time. The DWA emphasizes correct classifications of gestures performed at greater distances, reflecting the model’s robustness. DWA is defined as:

$$\text{DWA} = \frac{1}{K} \sum_{i=1}^K \mathbb{I}(\tilde{o}_i = o_i) w_i, \quad (9)$$

where,  $w_i = 1 + \beta \frac{\rho_i - \rho_{\min}}{\rho_{\max} - \rho_{\min}}$ ,  $\rho_i$  is the distance at which gesture  $i$  was performed,  $\rho_{\min} = 2 \text{ m}$  and  $\rho_{\max} = 30 \text{ m}$  are the minimum and maximum distances, respec-



tively,  $\beta = 1.6$  controls the weight for long distances, and  $\mathbb{I}(\tilde{o}_i = o_i)$  equals to 1 if the predicted label  $\tilde{o}_i$  matches the true label  $o_i$ , otherwise 0. While DWA evaluates the success rate with an emphasis on the farther cases, GSS measures the stability of predictions across the frames, ensuring consistent recognition. GSS is defined by

$$\text{GSS} = \frac{1}{K} \sum_{i=1}^K \left( \frac{1}{n_i} \sum_{j=n}^{n_i} \mathbb{I}(\tilde{o}_{i,j} = o_i) \right), \quad (10)$$

where  $n_i > n$  is the number of frames in video  $V_i$ ,  $\tilde{o}_{i,j}$  is the predicted label for sequence  $\{I_{j-n+1}, \dots, I_j\}$  in video  $V_i$ , and  $o_i$  is the true label for video  $V_i$ . A GSS value closer to one indicates a more stable prediction along the video. mAP provides an average measure of precision across all gesture classes, ensuring a balanced evaluation of the model’s capability.  $F_1$  Score is the harmonic mean of precision and recall, useful for evaluating models where both false positives and false negatives are impactful. These metrics provide a comprehensive evaluation of the DiG-Net model, focusing on accuracy, precision, and stability. Table 3 presents the comparative results after cross-validation, demonstrating the superior performance of the DiG-Net across all evaluation metrics, particularly in terms of recognition success rate.

Table 3: Evaluation results for different dynamic gesture recognition models

Model		Success rate (%)	DWA	GSS	$F_1$ score	mAP (%)	Inference Time (ms)
Swin	[65]	80.5	0.84	0.85	0.83	78.1	38
ViViT	[66]	78.3	0.82	0.84	0.80	77.5	44
TimeSformer	[67]	83.4	0.85	0.87	0.85	81.3	49
MViT	[68]	87.9	0.88	0.90	0.89	85.1	26
I3D	[69]	84.3	0.86	0.88	0.85	82.4	31
X3D	[70]	86.2	0.87	0.89	0.87	78.8	29
CorrNet	[71]	82.1	0.84	0.88	0.83	79.3	45
GestFormer	[72]	85.4	0.83	0.89	0.85	81.8	27
DiG-Net		97.3	0.92	0.96	0.93	94.9	35

### 3.4. DiG-Net analysis

We further analyze the performance of the proposed DiG-Net model. Figure 5 presents the gesture recognition success rate with respect to the distance  $\rho$  between the user and the camera. The success rate gradually decreases but remains relatively high in the desired range of up to 30 meters. This demonstrates the robustness of the DiG-Net model in recognizing gestures at hyper-range, though

performance diminishes as distance increases due to factors such as reduced resolution and increased visual noise. Figure 6 presents the confusion matrix for the DiG-Net model over the test data and for all 13 gesture classes. While some gestures may be visually similar, the temporal context modeling enabled by the Graph Transformer encoder and spatio-temporal graph structure helps disambiguate subtle motion patterns, reducing the likelihood of misclassification.

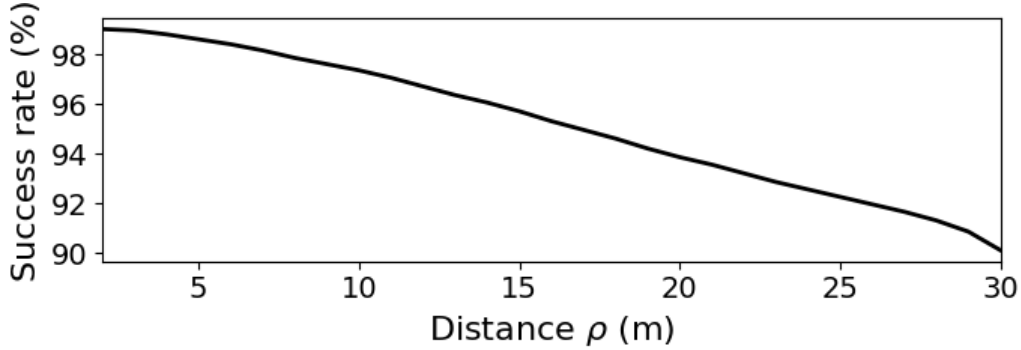


Figure 5: Gesture recognition success rate of the DiG-Net model with regard to the distance  $\rho$  of the user from the camera.

To understand the impact of the amount of training data on the success rate of gesture recognition, we analyzed the DiG-Net model’s performance with a varying number of labeled images. Figure 7 shows how the model’s average success rate improves as more labeled images are utilized. For each number of labeled images, the DiG-Net model was trained 10 times with different parts of the dataset, yielding an average success rate. The success rate of the model increases significantly, reaching 97.3% with the full dataset of 4,790 images. The gradual improvement with increased data demonstrates the model’s ability to learn complex gesture patterns effectively as more labeled examples are introduced, but also indicates that beyond a certain point, adding more data does not yield a substantial gain.

The above results were acquired with a video window length of up to  $n = 84$  frames. Hence, we now evaluate the performance of the DiG-Net with respect to the window length. The DiG-Net model was trained multiple times on video sequences  $V_t$  of varying lengths  $n$ , and each trained model’s performance was evaluated on test sequences of similar lengths. Figure 8 shows the recognition success rate of the DiG-Net with regard to the number of frames  $n$  in a video sample. First, with only one image of the gesture (i.e.,  $n = 1$ ), a poor recognition success rate of

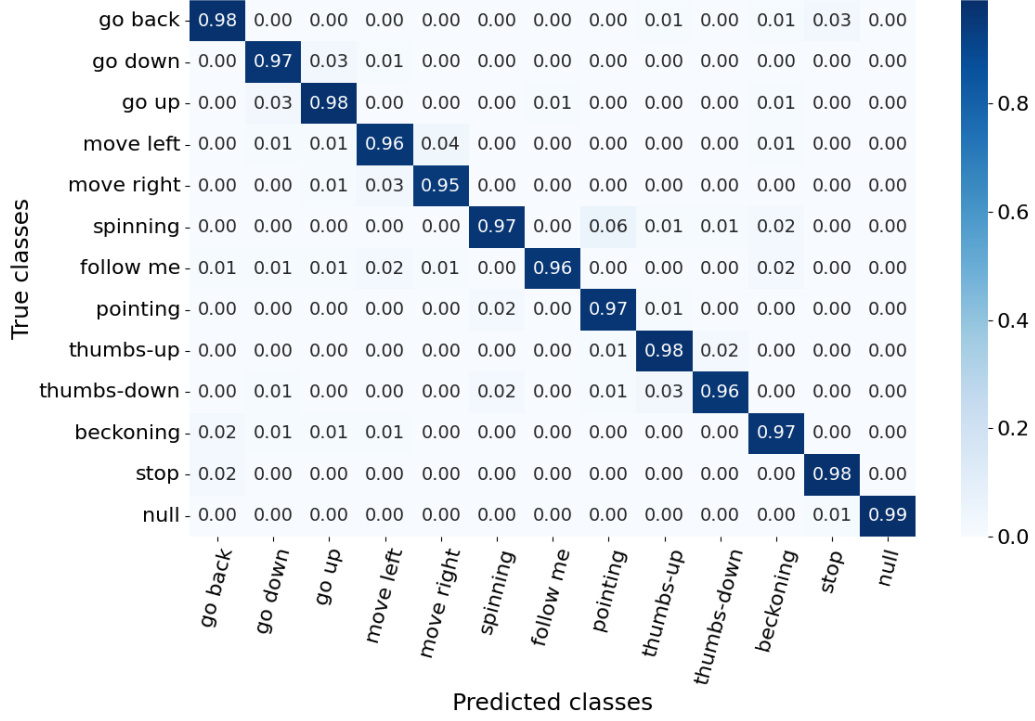


Figure 6: Confusion matrix for the gesture classification with the DiG-Net model across 13 gesture classes.

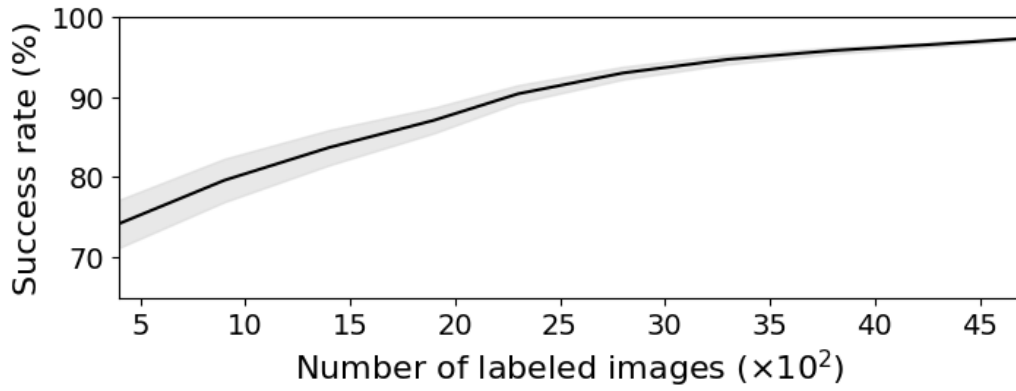
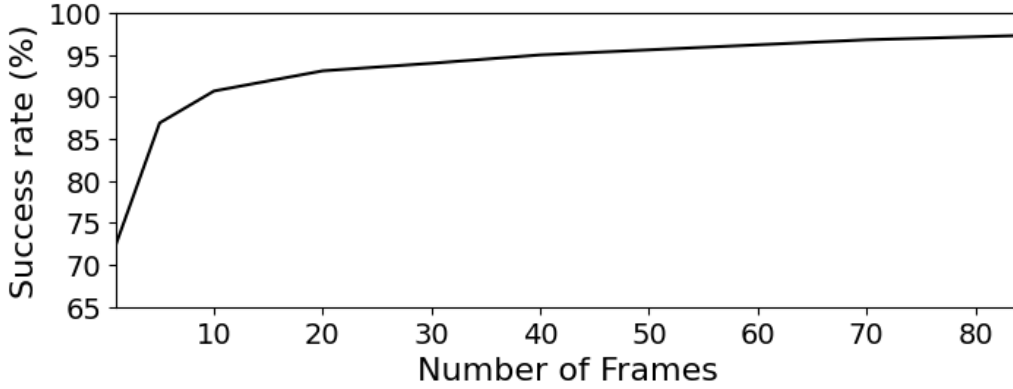


Figure 7: Gesture recognition success rate of the DiG-Net model with regard to the number of labeled training images.

Table 4: Ablation study results for DiG-Net components

Model Variant	Success rate (%)	DWA	GSS	$F_1$ score	mAP (%)
DiG-Net w/o DADA module	88.9	0.84	0.86	0.87	85.2
DiG-Net w/o STG module	89.7	0.85	0.88	0.88	86.4
DiG-Net w/o Graph Transformer	87.5	0.83	0.85	0.86	84.0
DiG-Net w/o RSTDAL	90.1	0.86	0.89	0.89	87.1
DiG-Net with short sequence	91.2	0.87	0.90	0.91	89.3
Full DiG-Net model	<b>97.3</b>	<b>0.92</b>	<b>0.96</b>	<b>0.93</b>	<b>94.9</b>

72.5% is achieved, due to the lack of dynamic information. As more frames are added to  $V_t$ , more dynamic information is included and the recognition improves. A longer video encapsulates more dynamic information on the exhibited gesture, yielding better recognition accuracy. However, increasing  $n$  may affect the time sensitivity and frequency of the recognition in real time. Nevertheless, increasing the sequence length beyond  $n = 84$  frames offers diminishing returns in terms of accuracy.

Figure 8: Gesture recognition success rate of the DiG-Net concerning the number of frames  $n$  in a video.

We further evaluate the data requirements for adding new gestures to the DiG-Net classifier. Starting with a DiG-Net model trained to classify eight gestures with a success rate of 98.6%, we examine the fine-tuning process needed to extend it to 13 gestures. Figure 9 shows the success rate of the expanded model as a function of the number of video clips used for fine-tuning, with each clip containing 84 frames. The results indicate that high accuracy is achieved with just 15

video examples, with only marginal gains beyond that point. This highlights the model’s ability to generalize and adapt to new gesture categories with minimal additional data.

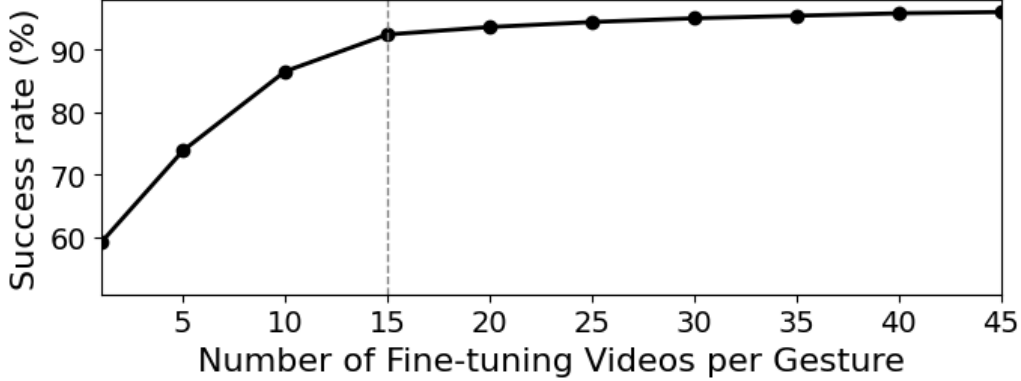


Figure 9: Success rate of the DiG-Net model after fine-tuning to recognize five additional gestures, plotted against the number of video clips used for fine-tuning (each clip spans 84 frames).

An ablation study was also conducted to evaluate the contribution of each component of the DiG-Net model to its overall performance. The study involved training and evaluating the model while removing a single component at a time, including the DADA module, STG module, Graph Transformer encoder, and the RSTDAL loss. In addition, we examined the impact of training with shorter video sequences by reducing the input length to  $n = 16$  frames. For the loss function ablation, we replaced the RSTDAL loss with the standard cross-entropy loss. The results are summarized in Table 4, demonstrating the importance of each component to the overall recognition accuracy, distance robustness, and temporal stability. The full DiG-Net model achieved the highest performance across all evaluation metrics, emphasizing the complementary contributions of depth-aware alignment, spatio-temporal graph reasoning, and global attention. Notably, removing the Graph Transformer or STG module resulted in a significant drop in accuracy and stability, while omitting the RSTDAL loss led to reduced emphasis on long-range gestures. Similarly, reducing the input sequence length limited the model’s ability to capture temporal dynamics. These results highlight the necessity of each module for robust gesture recognition under hyper-range conditions.

### 3.5. Sequence Analysis and Varying Conditions

To evaluate the robustness of the proposed DiG-Net model, we conducted a series of experiments involving complex gesture sequences and varying envi-

Table 5: Results of Sequence Analysis and Varying Conditions

Metric	Success rate (%)
Sequence accuracy	94.4%
Controlled lighting (Indoor)	96.8%
Bright sunlight (Outdoor)	93.1%
Overcast (Outdoor)	91.5%

ronmental conditions. In the first experiment, users performed complex gesture sequences consecutively, simulating real-world guidance scenarios for a robot. These sequences included various combinations of the 13 gesture classes. A total of 50 unique gesture sequences, each composed of 3 to 5 individual gestures, were used to ensure comprehensive testing. Table 5 presents the sequence accuracy, where a sequence is considered successful only if all gestures within it are correctly classified. The consistently high accuracy indicates that the DiG-Net model is capable of accurately interpreting and following multi-step gesture commands.

Additionally, we evaluated the model’s recognition accuracy under varying lighting conditions, including indoor controlled lighting, outdoor bright sunlight, and overcast outdoor settings. The recognition success rates are seen in Table 5. The high accuracy in controlled indoor environments demonstrates the model’s ability to recognize gestures under optimal conditions, while the slightly lower accuracy in outdoor environments reflects the challenges posed by changing lighting and environmental noise. Nevertheless, these results demonstrate the model’s robustness in adapting to different environmental conditions, ensuring reliable performance in diverse real-world scenarios.

### 3.6. Robustness and Inference Efficiency

To further evaluate DiG-Net’s suitability for practical assistive robotics applications, we conducted experiments focused on robustness to environmental noise, real-time performance, and synthetic optical degradation. These tests simulate critical aspects of real-world assistive scenarios, ensuring the model maintains high reliability under challenging operational conditions.

**Robustness to Environmental Noise:** Assistive robotic systems frequently operate in dynamic and cluttered environments where irrelevant movements, background clutter, and sudden visual interferences occur frequently. To evaluate DiG-Net’s robustness, we artificially injected background clutter, dynamic interference

from moving objects, and abrupt lighting changes into existing recorded gesture sequences. Table 6 presents the recognition accuracy under different noise intensities.

Table 6: Recognition Accuracy under Environmental Noise Conditions

Condition	Success rate (%)
Mild clutter/interference	95.8%
Moderate clutter/interference	93.5%
Severe clutter/interference	90.1%

**Real-Time Processing Simulation:** Real-time responsiveness is crucial in assistive scenarios, as delayed system reactions may lead to user frustration or incorrect robotic responses. We simulated real-time conditions by measuring inference speed in frames per second (FPS) on video sequences of varying length. Table 7 summarizes the inference performance. Results confirm that the model supports real-time recognition even with longer input sequences.

Table 7: Inference Speed under Real-Time Simulation

Sequence Length	Inference Speed (FPS)
8-frame sequence	28
16-frame sequence	24
32-frame sequence	19
84-frame sequence	12

**Synthetic Optical Degradation:** To simulate realistic environmental challenges such as fog, defocus, or motion blur, we synthetically degraded gesture videos using Gaussian blur, motion blur, and synthetic fog effects at varying intensities. Table 8 presents the model’s accuracy under these visual degradations.

Table 8: Recognition Accuracy under Optical Degradation

Degradation Level	Success rate (%)
Mild blur/fog	94.7%
Moderate blur/fog	91.2%
Severe blur/fog	88.3%

## 4. Conclusions

In this work, we proposed DiG-Net, a model for recognizing dynamic hand gestures at hyper-range distances of up to 30 meters using a monocular RGB camera. The model tackles key challenges in assistive robotics, including visual degradation, physical attenuation, and environmental noise in both indoor and outdoor settings. DiG-Net integrates DADA modules, spatio-temporal graph reasoning, and Graph Transformer encoders to capture spatial distortions and long-range temporal dependencies. We also introduced the RSTDAL loss, which adapts the decision margin based on distance and motion, improving recognition at extended ranges. Our experiments show that DiG-Net outperforms prior methods, achieving 97.3% accuracy under challenging conditions.

The model significantly enhances the quality of life and independence for individuals with mobility impairments by enabling intuitive, long-range interaction with robotic assistants across various environments, including home healthcare, industrial safety, and emergency response. Future work will aim at expanding the assistive gesture vocabulary, integrating non-intentional body language cues, improving real-time responsiveness, and enhancing robustness to highly dynamic and crowded environments, thus further broadening the impact and usability of assistive robotic technologies.

## Declaration of competing interest

The authors declare that they have no known competing financial interests or personal relationships that could have appeared to influence the work reported in this paper.

## Funding

This work was supported by the Israel Innovation Authority (grant No. 77857).

## References

- [1] A. Nanavati, V. Ranganeni, M. Cakmak, Physically assistive robots: A systematic review of mobile and manipulator robots that physically assist people with disabilities, *Annual Review of Control, Robotics, and Autonomous Systems* 7 (2023).



- [2] L. Leal-Taixé, S. Roth, Computer Vision–ECCV 2018 Workshops: Munich, Germany, September 8–14, 2018, Proceedings, Part VI, Vol. 11134, Springer, 2019.
- [3] N. Robinson, B. Tidd, D. Campbell, D. Kulić, P. Corke, Robotic vision for human-robot interaction and collaboration: A survey and systematic review, *ACM Transactions on Human-Robot Interaction* 12 (1) (2023) 1–66.
- [4] S. Drolshagen, M. Pfingsthorn, A. Hein, Context-aware robotic assistive system: Robotic pointing gesture-based assistance for people with disabilities in sheltered workshops, *Robotics* 12 (5) (2023) 132.
- [5] P. A. Lasota, T. Fong, J. A. Shah, et al., A survey of methods for safe human-robot interaction, *Foundations and Trends® in Robotics* 5 (4) (2017) 261–349.
- [6] M. Safeea, P. Neto, Minimum distance calculation using laser scanner and imus for safe human-robot interaction, *Robotics and Computer-Integrated Manufacturing* 58 (2019) 33–42.
- [7] D. P. Losey, C. G. McDonald, E. Battaglia, M. K. O’Malley, A review of intent detection, arbitration, and communication aspects of shared control for physical human–robot interaction, *Applied Mechanics Reviews* 70 (1) (2018) 010804.
- [8] S. Frennert, J. Persson, S. Skavron, A critical narrative review of assistive robotics and call for a systems and user-centered approaches to enhance quality of life of individuals with disabilities, in: *Adjunct Proceedings of the 2024 Nordic Conference on Human-Computer Interaction*, 2024, pp. 1–11.
- [9] E. S. Shourmasti, R. Colomo-Palacios, H. Holone, S. Demi, User experience in social robots, *Sensors* 21 (15) (2021) 5052.
- [10] M. A. Goodrich, A. C. Schultz, et al., Human–robot interaction: a survey, *Foundations and Trends in Human–Computer Interaction* 1 (3) (2008) 203–275.
- [11] I. Maurtua, I. Fernandez, A. Tellaeché, J. Kildal, L. Susperregi, A. Ibar-guren, B. Sierra, Natural multimodal communication for human–robot col-laboration, *International Journal of Advanced Robotic Systems* 14 (4) (2017) 1729881417716043.

- [12] M. J. Matarić, Socially assistive robotics: Human augmentation versus automation, *Science Robotics* 2 (4) (2017) eaam5410.
- [13] R. G. Boboc, A. I. Dumitru, C. Antonya, Point-and-command paradigm for interaction with assistive robots, *International Journal of Advanced Robotic Systems* 12 (6) (2015) 75.
- [14] M. A. Haseeb, M. Kyrarini, S. Jiang, D. Ristic-Durrant, A. Gräser, Head gesture-based control for assistive robots, in: *Proceedings of the 11th Pervasive Technologies Related to Assistive Environments Conference*, 2018, pp. 379–383.
- [15] N. Rudigkeit, M. Gebhard, Amicus—a head motion-based interface for control of an assistive robot, *Sensors* 19 (12) (2019) 2836.
- [16] J. Yang, K. Shibata, D. Weber, Z. Erickson, High-density electromyography for effective gesture-based control of physically assistive mobile manipulators, *npj Robotics* 3 (1) (2025) 2.
- [17] M. Ababneh, H. Sha’ban, D. AlShalabe, D. Khader, H. Mahameed, M. AlQudimat, Gesture controlled mobile robotic arm for elderly and wheelchair people assistance using kinect sensor, in: *2018 15th International Multi-Conference on Systems, Signals & Devices (SSD)*, IEEE, 2018, pp. 636–641.
- [18] P. Neto, M. Simão, N. Mendes, M. Safeea, Gesture-based human-robot interaction for human assistance in manufacturing, *The International Journal of Advanced Manufacturing Technology* 101 (2019) 119–135.
- [19] C. Werner, N. Kardaris, P. Koutras, A. Zlatintsi, P. Maragos, J. M. Bauer, K. Hauer, Improving gesture-based interaction between an assistive bathing robot and older adults via user training on the gestural commands, *Archives of gerontology and geriatrics* 87 (2020) 103996.
- [20] G. F. Muñoz, R. A. M. Cardenas, F. Pla, A kinect-based interactive system for home-assisted active aging, *Sensors* 21 (2) (2021) 417.
- [21] M. Oudah, A. Al-Naji, J. Chahl, Elderly care based on hand gestures using kinect sensor, *Computers* 10 (1) (2020) 5.

- [22] H. R. T. Bandara, K. Priyanayana, A. B. P. Jayasekara, D. Chandima, R. Gopura, An intelligent gesture classification model for domestic wheelchair navigation with gesture variance compensation, *Applied bionics and biomechanics* 2020 (1) (2020) 9160528.
- [23] Q. Gao, J. Liu, Z. Ju, Robust real-time hand detection and localization for space human–robot interaction based on deep learning, *Neurocomputing* 390 (2020) 198–206.
- [24] X. Wang, H. Shen, H. Yu, J. Guo, X. Wei, Hand and arm gesture-based human-robot interaction: A review, in: *International Conference on Algorithms, Computing and Systems*, 2022, pp. 1–7.
- [25] J. Urakami, K. Seaborn, Nonverbal cues in human–robot interaction: A communication studies perspective, *ACM Transactions on Human-Robot Interaction* 12 (2) (2023) 1–21.
- [26] J. P. Wachs, M. Kölsch, H. Stern, Y. Edan, Vision-based hand-gesture applications, *Commun. ACM* 54 (2) (2011) 60–71.
- [27] E. Bamani, E. Nissinman, L. Koenigsberg, I. Meir, Y. Matalon, A. Sintov, Recognition and estimation of human finger pointing with an RGB camera for robot directive (2023). [arXiv:2307.02949](https://arxiv.org/abs/2307.02949).
- [28] K. Zhang, Z. Yu, D. Zhang, Z. Wang, B. Guo, Racon: A gesture recognition approach via doppler radar for intelligent human-robot interaction, in: *IEEE international conference on pervasive computing and communications workshops (PerCom Workshops)*, 2020, pp. 1–6.
- [29] J. Yu, M. Li, X. Zhang, T. Zhang, X. Zhou, A multi-sensor gesture interaction system for human-robot cooperation, in: *IEEE International Conference on Networking, Sensing and Control (ICNSC)*, Vol. 1, 2021, pp. 1–6.
- [30] J. Yu, M. Qin, S. Zhou, Dynamic gesture recognition based on 2D convolutional neural network and feature fusion, *Scientific Reports* 12 (2022) 4345. [doi:10.1038/s41598-022-08133-z](https://doi.org/10.1038/s41598-022-08133-z).
- [31] K. Nickel, R. Stiefelhagen, Visual recognition of pointing gestures for human–robot interaction, *Image and vision computing* 25 (12) (2007) 1875–1884.

- [32] L. Zhou, C. Du, Z. Sun, T. L. Lam, Y. Xu, Long-range hand gesture recognition via attention-based ssd network, in: IEEE International Conference on Robotics and Automation (ICRA), 2021, pp. 1832–1838. doi: 10.1109/ICRA48506.2021.9561189.
- [33] H. Liang, L. Fei, S. Zhao, J. Wen, S. Teng, Y. Xu, Mask-guided multiscale feature aggregation network for hand gesture recognition, *Pattern Recognition* 145 (2024) 109901.
- [34] Y. Kim, C. Moon, Non-contact gesture recognition using the electric field disturbance for smart device application, *International Journal of Multimedia and Ubiquitous Engineering* 9 (2) (2014) 133–140.
- [35] G. Canal, C. Angulo, S. Escalera, Gesture based human multi-robot interaction, in: IEEE International Joint Conference on Neural Networks (IJCNN), 2015, pp. 1–8.
- [36] X. Shen, H.-S. Kim, S. Komatsu, A. Markman, B. Javidi, An overview of spatial-temporal human gesture recognition under degraded environments using integral imaging, *Three-Dimensional Imaging, Visualization, and Display* 2019 10997 (2019) 161–167.
- [37] F. Pla, P. Latorre-Carmona, E. Salvador-Balaguer, B. Javidi, Three-dimensional integral imaging for gesture recognition under occlusions, in: *Computational Imaging III*, Vol. 10669, SPIE, 2018, pp. 14–19.
- [38] E. Bamani, E. Nissinman, I. Meir, L. Koenigsberg, A. Sintov, Ultra-range gesture recognition using a web-camera in human-robot interaction, *Eng. Applications of Artificial Intelligence* (In press, 2024).
- [39] S. Kang, B. Tversky, From hands to minds: Gestures promote understanding, *Cognitive Research: Principles and Implications* 1 (2016) 4. doi: 10.1186/s41235-016-0004-9.
- [40] S. Clough, M. C. Duff, The role of gesture in communication and cognition: Implications for understanding and treating neurogenic communication disorders, *Frontiers in Human Neuroscience* 14 (2020) 323.
- [41] D. Xu, X. Wu, Y.-L. Chen, Y. Xu, Online dynamic gesture recognition for human robot interaction, *Journal of Intelligent & Robotic Systems* 77 (3) (2015) 583–596.

- [42] X. Ma, J. Peng, Kinect sensor-based long-distance hand gesture recognition and fingertip detection with depth information, *Journal of Sensors* 2018 (1) (2018) 5809769.
- [43] R. Kabir, N. Ahmed, N. Roy, M. R. Islam, A novel dynamic hand gesture and movement trajectory recognition model for non-touch hri interface, in: *IEEE Eurasia Conference on IOT, Communication and Engineering (ECICE)*, 2019, pp. 505–508.
- [44] J. Bokstaller, C. M. Improta, Dynamic gesture recognition, *arXiv preprint arXiv:2109.09396* (2021).
- [45] Q. Gao, Y. Chen, Z. Ju, Y. Liang, Dynamic hand gesture recognition based on 3d hand pose estimation for human–robot interaction, *IEEE Sensors Journal* 22 (18) (2022) 17421–17430.
- [46] C. Yi, L. Zhou, Z. Wang, Z. Sun, C. Tan, Long-range hand gesture recognition with joint ssd network, in: *IEEE International Conference on Robotics and Biomimetics*, 2018, pp. 1959–1963. doi:10.1109/ROBIO.2018.8665302.
- [47] C. C. dos Santos, J. L. A. Samatelo, R. F. Vassallo, Dynamic gesture recognition by using cnns and star rgb: A temporal information condensation, *Neurocomputing* 400 (2020) 238–254.
- [48] K. R. Pyun, K. Kwon, M. J. Yoo, K. K. Kim, D. Gong, W.-H. Yeo, S. Han, S. H. Ko, Machine-learned wearable sensors for real-time hand-motion recognition: toward practical applications, *National Science Review* 11 (2) (2023) nwad298.
- [49] R. Tchantchane, H. Zhou, S. Zhang, G. Alici, A review of hand gesture recognition systems based on noninvasive wearable sensors, *Advanced Intelligent Systems* 5 (10) (2023) 2300207.
- [50] T.-H. Tran, H.-N. Tran, H.-G. Doan, Dynamic hand gesture recognition from multi-modal streams using deep neural network, in: *International conference on multi-disciplinary trends in artificial intelligence*, Springer, 2019, pp. 156–167.

- [51] D. Wu, L. Pigou, P.-J. Kindermans, N. D.-H. Le, L. Shao, J. Dambre, J.-M. Odobez, Deep dynamic neural networks for multimodal gesture segmentation and recognition, *IEEE transactions on pattern analysis and machine intelligence* 38 (8) (2016) 1583–1597.
- [52] S. Ji, W. Xu, M. Yang, K. Yu, 3d convolutional neural networks for human action recognition, *IEEE transactions on pattern analysis and machine intelligence* 35 (1) (2012) 221–231.
- [53] S. Yan, Y. Xiong, D. Lin, Spatial temporal graph convolutional networks for skeleton-based action recognition, in: *Proceedings of the AAAI conference on artificial intelligence*, Vol. 32, 2018.
- [54] C. Godard, O. Mac Aodha, M. Firman, G. J. Brostow, Digging into self-supervised monocular depth estimation, in: *Proceedings of the IEEE/CVF international conference on computer vision*, 2019, pp. 3828–3838.
- [55] Z. Ren, J. Meng, J. Yuan, Z. Zhang, Robust hand gesture recognition with kinect sensor, in: *ACM international conference on Multimedia*, 2011, pp. 759–760.
- [56] K. Gao, H. Zhang, X. Liu, X. Wang, L. Xie, B. Ji, Y. Yan, E. Yin, Challenges and solutions for vision-based hand gesture interpretation: A review, *Computer Vision & Image Understanding* (2024) 104095.
- [57] A. Bonci, P. D. Cen Cheng, M. Indri, G. Nabissi, F. Sibona, Human-robot perception in industrial environments: A survey, *Sensors* 21 (5) (2021) 1571.
- [58] T. K. Mohd, N. Nguyen, A. Y. Javaid, Multi-modal data fusion in enhancing human-machine interaction for robotic applications: a survey, *arXiv preprint arXiv:2202.07732* (2022).
- [59] K. He, X. Zhang, S. Ren, J. Sun, Deep residual learning for image recognition, in: *IEEE Conference on Computer Vision and Pattern Recognition*, 2016, pp. 770–778.
- [60] J. Redmon, A. Farhadi, YOLOv3: An incremental improvement (2018). [arXiv:1804.02767](https://arxiv.org/abs/1804.02767).
- [61] D. F. Swinehart, The beer-lambert law, *Journal of chemical education* 39 (7) (1962) 333.

- [62] R. Liaw, E. Liang, R. Nishihara, P. Moritz, J. E. Gonzalez, I. Stoica, Tune: A research platform for distributed model selection and training, arXiv preprint arXiv:1807.05118 (2018).
- [63] X. Chen, C. Liang, D. Huang, E. Real, K. Wang, H. Pham, X. Dong, T. Luong, C.-J. Hsieh, Y. Lu, et al., Symbolic discovery of optimization algorithms, *Advances in neural information processing systems* 36 (2023) 49205–49233.
- [64] R. Liaw, E. Liang, R. Nishihara, P. Moritz, J. E. Gonzalez, I. Stoica, Tune: A research platform for distributed model selection and training, arXiv preprint arXiv:1807.05118 (2018).
- [65] Z. Liu, J. Ning, Y. Cao, Y. Wei, Z. Zhang, S. Lin, H. Hu, Video swin transformer, arXiv preprint arXiv:2106.13230 (2022) 3192–3201.
- [66] A. Arnab, M. Dehghani, G. Heigold, C. Sun, M. Lucic, C. Schmid, ViViT: A video vision transformer, in: *IEEE/CVF International Conference on Computer Vision (ICCV)*, 2021, pp. 6816–6826.
- [67] G. Bertasius, H. Wang, L. Torresani, Is space-time attention all you need for video understanding?, in: *International Conference on Machine Learning (ICML)*, 2021.
- [68] H. Fan, B. Xiong, K. Mangalam, Y. Li, Z. Yan, J. Malik, C. Feichtenhofer, Multiscale vision transformers, in: *ICCV*, 2021.
- [69] J. Carreira, A. Zisserman, Quo vadis, action recognition? a new model and the kinetics dataset, in: *IEEE Conference on Computer Vision and Pattern Recognition*, 2017, pp. 6299–6308.
- [70] C. Feichtenhofer, X3D: Expanding architectures for efficient video recognition, in: *IEEE/CVF Conference on Computer Vision and Pattern Recognition (CVPR)*, 2020, pp. 200–210.
- [71] L. Hu, L. Gao, Z. Liu, W. Feng, Continuous sign language recognition with correlation network, in: *Proceedings of the IEEE/CVF Conference on Computer Vision and Pattern Recognition*, 2023, pp. 2529–2539.
- [72] M. Garg, D. Ghosh, P. M. Pradhan, Gestformer: Multiscale wavelet pooling transformer network for dynamic hand gesture recognition, in: *Proceedings*

of the IEEE/CVF Conference on Computer Vision and Pattern Recognition,  
2024, pp. 2473–2483.